O. L. Phillips and A. H. Gentry, *Science* **263**, 954 (1994); R. A. Houghton, *Tellus Ser. B* **48**, 420 (1996); R. F. Keeling, S. C. Piper, M. Heimann, *Nature* **381**, 218 (1996).
31. R. B. McKane, E. B. Rastetter, J. M. Melillo, G. R. Shaver, C. S. Hopkinson, *Global Biogeochem. Cycles* **9**, 329 (1995); Ch. Korner and F. A. Bazzaz, Eds., *Carbon Dioxide, Populations, and Communities* (Academic Press, San Diego, 1996); J. Lloyd and G. D. Farquhar, *Funct. Ecol.* **10**, 4 (1996).
32. R. Swap, M. Garstang, S. Greco, R. Talbot, P. Kallberg, *Tellus Ser. B* **44**, 133 (1992).
33. For example, D. S. Schimel *et al.*, *Global Biogeochem. Cycles* **10**, 677 (1996); P. M. Vitousek *et al.*, *Ecol. Appl.* **7**, 737 (1997). Tropical forest tree growth has been shown experimentally to increase after N and P fertilization [E. V. J. Tanner, V. Kapos, W. Franco, *Ecology* **73**, 78 (1992)].
34. We assumed that: (i) 48% of biomass is in the form of C {based on burning experiments near Manaus, central Amazonia [J. A. Carvalho Jr., J. M. Santos, J. C. Santos, M. M. Leitão, N. Higuchi, *Atmos. Environ.* **29**, 2301 (1995); J. A. Carvalho Jr., N. Higuchi, T. M. Araujo, J. C. Santos, *J. Geophys. Res.* **103**, 13195 (1998)]}; (ii) that the ratio of aboveground biomass to root biomass is 3:1 {the average value of three studies in Brazilian Amazonia [P. Fearnside, *Emissão e Sequestro de CO_2* (Companha Vale do Rio Doce, Rio de Janeiro, 1994), pp. 95–124]}, consistent with a global analysis of root biomass allocation [M. A. Cairns, S. Brown, E. Helmer, G. Baumgardner, *Oecologia* **111**, 1 (1997)]; and (iii) that root biomass increased in proportion to aboveground biomass. We ignored C stocks in fine litter, dead wood, and soil, which may also have changed.
35. Although PSP data address the problem of spatial variability that can limit extrapolation of eddy covariance studies, they clearly cannot assess the behavior of necromass and belowground C pools, which might be expected to increase together with biomass. A combination of eddy covariance and biomass studies may provide a useful tool in the future to examine belowground processes.
36. The "missing" sink was recently estimated at ~1.4 Gt [D. S. Schimel, *Global Change Biol.* **1**, 77 (1995)]. By comparison, deforestation in Brazilian Amazonia was estimated to yield a net C emission of 0.34 Gt in 1990 [P. M. Fearnside, in *Biomass Burning in South America, Southeast Asia, and Temperate and Boreal Ecosystems, and the Oil Fires of Kuwait*, J. S. Levine, Ed. (MIT Press, Cambridge, MA, 1996), pp. 606–617]. Deforestation in the whole Neotropics was estimated to yield 0.6 ± 0.3 Gt C annually between 1980 and 1990 [R. A. Houghton, in *Forest Ecosystems, Forest Management and the Global Carbon Cycle*, M. G. Apps and D. T. Price, Eds., *NATO ASI Ser. I Global Environ. Change*, vol. 40 (Springer-Verlag, Heidelberg, Germany, 1996)].
37. W. F. Laurance, *Trends Ecol. Evol.*, in press.
38. E. Salati and C. A. Nobre, *Clim. Change* **19**, 177 (1991); A. Kattenberg *et al.* (1996), *Climate Change* (Intergovernmental Panel on Climate Change/Cambridge Univ. Press, Cambridge, 1995), pp. 285–357.
39. D. Z. Sun, *Geophys. Res. Lett.* **24**, 2031 (1997).
40. We gratefully acknowledge help in Peru from the late A. H. Gentry, as well as M. Aguilar, C. Díaz, C. Grández, N. Jaramillo, M. Jarrell, K. Johnson, D. Milanowski, R. Ortíz, S. Rose, J. Terborgh, A. Vásquez, and the logistical support of INRENA, ACEER, Cuzco Amazonico Lodge, Explorama Tours, Instituto de Investigaciones de la Amazonía Peruana, Peruvian Safaris, Universidad Nacional de la Amazonía Peruana (Iquitos), and Universidad Nacional de San Antonio Abad del Cusco (Cusco and Puerto Maldonado). In Brazil, we acknowledge the help of R. J. Ribeiro, Y. Biot, P. Delamonica, C. Gascon, and other BIONTE and BDFFP project members. We thank J. Terborgh, R. Foster, R. Condit, S. Lao, S. P. Hubbell, M. D. Swaine, D. Nicholson, R. Keenan, T. Richards, J. N. M. Silva, J. P. Veillon, J. Comiskey, and R. Moraes de Jesus for kindly making data available and for other help. Peruvian field research was supported by the American Philosophical Society, National Geographic Society (grant 5472-95), NSF (BSR-9001051), World Wide Fund for Nature (WWF)–U.S./Garden Club of America, Conservation International, the MacArthur and Mellon Foundations, Missouri Botanical Garden, and a Research Fellowship from the U.K. Natural Environment Research Council (NERC). Support for Venezuelan data analysis was provided by a cooperative agreement between the USDA Southern Forest Experiment Station and the University of Illinois (grant 19-91-064). The Biological Dynamics of Forest Fragments Project (BDFFP) was supported by WWF-US, INPA, Smithsonian Institution, and the MacArthur and Mellon Foundations. Work by Y.M., N.H., and J.G. formed part of the Biomass and Nutrient Experiment (BIONTE) and the Anglo-Brazilian Climate Observation Study (ABRACOS), supported by the U.K. Overseas Development Administration in collaboration with the Agencia Brasileira de Cooperação, and aided by a NERC Terrestrial Initiative in Global and Environmental Research (TIGER) grant.

13 January 1998; accepted 11 September 1998

A Large Terrestrial Carbon Sink in North America Implied by Atmospheric and Oceanic Carbon Dioxide Data and Models

S. Fan, M. Gloor, J. Mahlman, S. Pacala, J. Sarmiento, T. Takahashi, P. Tans

Atmospheric carbon dioxide increased at a rate of 2.8 petagrams of carbon per year (Pg C year^{-1}) during 1988 to 1992 (1 Pg = 10^{15} grams). Given estimates of fossil carbon dioxide emissions, and net oceanic uptake, this implies a global terrestrial uptake of 1.0 to 2.2 Pg C year^{-1}. The spatial distribution of the terrestrial carbon dioxide uptake is estimated by means of the observed spatial patterns of the greatly increased atmospheric carbon dioxide data set available from 1988 onward, together with two atmospheric transport models, two estimates of the sea-air flux, and an estimate of the spatial distribution of fossil carbon dioxide emissions. North America is the best constrained continent, with a mean uptake of 1.7 ± 0.5 Pg C year^{-1}, mostly south of 51 degrees north. Eurasia–North Africa is relatively weakly constrained, with a mean uptake of 0.1 ± 0.6 Pg C year^{-1}. The rest of the world's land surface is poorly constrained, with a mean source of 0.2 ± 0.9 Pg C year^{-1}.

A number of carbon cycle studies conducted in the last decade have indicated that the oceans and terrestrial ecosystems in the Northern Hemisphere absorb atmospheric CO_2 at a rate of about 3 Pg C year^{-1} (*1–3*). Atmospheric CO_2 concentrations in the Northern Hemisphere are about 3 parts per million (ppm, mole fraction in dry air) greater than those in the Southern Hemisphere. Fossil CO_2 is released predominantly at northern latitudes (Table 1), which should result in a north-to-south decrease of 4 to 5 ppm in the concentration of atmospheric CO_2 (*4*). A Northern Hemisphere sink is implied because the observed gradient is smaller than this. The original studies disagreed on whether the sink was predominantly oceanic (*1*) or terrestrial (*2*). Recent studies with atmospheric $^{13}C/^{12}C$ ratios (*5*) and oxygen concentrations (*6*) concluded that the sink is caused primarily by terrestrial biosphere uptake. Other studies demonstrated increased activity of sufficient magnitude by the terrestrial biosphere in northern latitudes: a longer growing season observed in satellite measurements of surface color (*7*) and an increase over time of the amplitude of the annual cycle of atmospheric CO_2 concentrations caused by terrestrial vegetation (*8*).

The partitioning of the Northern Hemisphere terrestrial CO_2 sources and sinks between Eurasia and North America may be estimated by using the west-to-east gradient of atmospheric CO_2 across the continents. The west-east signal is much smaller and more difficult to detect than the north-south signal for two reasons. First, the CO_2 distribution is smoothed more by the relatively rapid zonal atmospheric transport than by the slower meridional transport (weeks instead of ~1 year for interhemispheric exchange). Sec-

S. Fan and J. Sarmiento, Atmospheric and Oceanic Sciences Program, Princeton University, Princeton, NJ 08544, USA. M. Gloor and S. Pacala, Department of Ecology and Evolutionary Biology, Princeton University, Princeton, NJ 08542, USA. J. Mahlman, Geophysical Fluid Dynamics Laboratory–National Oceanic and Atmospheric Administration (NOAA), Princeton University, Post Office Box 308, Princeton, NJ 08542, USA. T. Takahashi, Lamont-Doherty Earth Observatory, Columbia University, Palisades, NY 10964, USA. P. Tans, Climate Modeling and Diagnostics Laboratory, NOAA, Boulder, CO 80303, USA.

*Correspondence should be addressed to the Carbon Modeling Consortium, AOS Program, Princeton University, Princeton, NJ 08544, USA. E-mail: cmc@princeton.edu

ond, atmospheric sampling stations have traditionally been located primarily offshore, away from the largest terrestrial signals to avoid the complexities associated with continental atmospheric boundary layers, the diurnal character of photosynthesis, local fossil fuel emissions, and topography (Fig. 1).

To provide improved estimates of net annual terrestrial sources and sinks, we have developed an inverse model. Let $O(\mathbf{x})$ be the annual-average spatial pattern of atmospheric CO_2 caused by atmospheric transport acting on the sea-air CO_2 flux, and $F(\mathbf{x})$ and $R(\mathbf{x})$ be the corresponding annual-average spatial patterns associated with fossil fuel emissions and the seasonal rectification, respectively (where $\mathbf{x}$ is the spatial coordinate vector). Seasonal rectification results from the correlation between the seasonality of vertical mixing in the atmosphere and the seasonality of photosynthesis and respiration in the land biosphere, which causes gradients in the annual mean CO_2 concentration even when the terrestrial biosphere has no net annual emissions (*9*). Assuming a terrestrial biosphere with no net emissions, the expected annual average spatial pattern of atmospheric CO_2 is $O(\mathbf{x}) + F(\mathbf{x}) + R(\mathbf{x})$. We use the difference between this expected spatial pattern and the observed annual average concentrations of atmospheric CO_2 at sampling stations [$S(\mathbf{x}_j)$ for a station located at $\mathbf{x}_j$] to estimate the magnitude and spatial distribution of terrestrial uptake.

We divide the land surface into N regions and let $b_i(\mathbf{x})$ be the global spatial pattern of atmospheric CO_2 caused by atmospheric transport acting on a standard annual terrestrial uptake of 1 Pg C within the i^{th} region. Then, the total spatial pattern caused by nonzero terrestrial uptake is

$$B(\mathbf{x}) = \sum_{i=1}^{N} \alpha_i b_i(\mathbf{x}) \quad (1)$$

where α_i is the magnitude in Pg C year^{-1} of terrestrial uptake in the i^{th} region, and is estimated by linear regression (*10*).

We used two separate atmospheric transport models of the Geophysical Fluid Dynamics Laboratory (GFDL) to calculate the expected spatial pattern of atmospheric CO_2. A previous model comparison study showed significant differences in predictions of the fossil CO_2 distribution and rectification effect (*4*). The use of two different models gives us some measure of the sensitivity of the results to differences in the transport model. The Global Chemical Transport Model (GCTM) uses winds generated previously by an atmospheric general circulation model (*11*, *12*). In contrast, the SKYHI model (*12*, *13*) calculates tracer transport at the same time it calculates the winds and subgrid-scale mixing.

To calculate the $O(\mathbf{x})$ function, we used two different estimates of the global spatiotemporal distribution of net sea-air CO_2 flux. OBM is an annual mean sea-air flux from a global ocean biogeochemistry model (*14*). T97 is a seasonally resolved sea-air flux field based on estimates from the more than 2.1 million measurements of the sea-air difference of CO_2 partial pressure (pCO_2) gathered over the last three decades and interpolated by using annual mean ocean currents from OBM (*15*, *16*). Pacific equatorial (10°N to 10°S) observations made during El Niño periods were excluded from the estimate. The data are normalized to 1990. The total sea-air CO_2 flux is larger in OBM than T97 (Table 1). A comparison of model simulations with observations of $\Delta^{14}C$ in the ocean favors the larger uptake of OBM (*17*).

The two atmospheric models and two patterns of sea-air CO_2 flux gave us four possible combinations. To calculate in each case, we ran the atmospheric model with the prescribed pattern of sea-air flux for five annual cycles until the annual average spatial distribution of atmospheric CO_2 reached a steady state.

To calculate $O(\mathbf{x})$, we used data on national fossil fuel consumption distributed with the same spatial distribution as population density (*18*). Using this pattern of release at the surface, we ran each atmospheric model to its steady state as above.

Finally, to calculate $R(\mathbf{x})$ and the $b_i(\mathbf{x})$, a

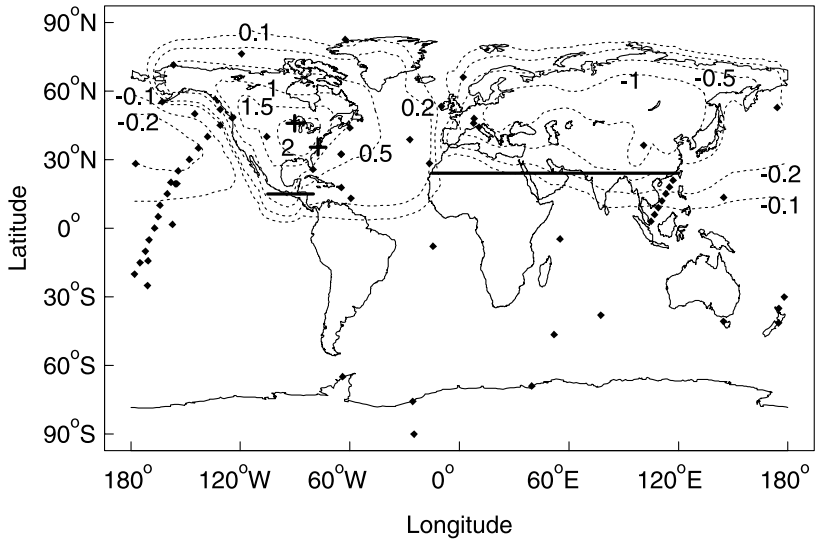

Fig. 1. A map of the atmospheric CO_2 sampling network. Sites are shown as solid diamonds. (The Globalview labels for the Northern Hemisphere stations are given in the legend of Fig. 3). The tall tower sites are shown as crosses. The thick horizontal lines divide the land surfaces into three regions where terrestrial carbon uptake has been estimated: North America, Eurasia–North Africa, and Tropics and Southern Hemisphere. The dotted contour lines show the difference between predicted surface CO_2 concentrations (ppm) with estimated terrestrial uptake and with North American terrestrial uptake set to zero (model results are shown for GCTM with the T97 sea-air fluxes).

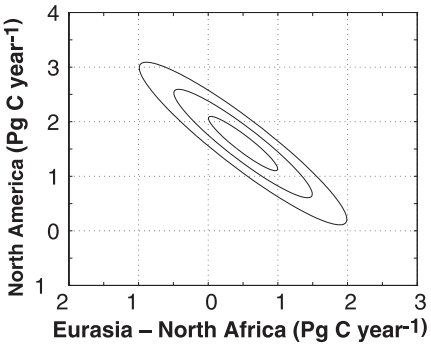

Fig. 2. Inversion uncertainties for North American terrestrial uptake versus Eurasia–North African terrestrial uptake. Ellipses of 1, 2, and 3 SDs are shown.

Table 1. Regional distribution of fossil CO_2 emissions and sea-air fluxes for 1990. T97 and OBM are two different air-sea flux estimates (see text).

Region	Fossil emissions (Pg C year^{-1})
North America (>15°N)	1.6
Eurasia and North Africa (>24°N)	3.6
Tropics and Southern Hemisphere	0.7
Total	5.9

	Ocean uptake (Pg C year^{-1})	
	T97	OBM
North Atlantic (>15°N)	0.55	0.51
North Pacific (>15°N)	0.29	0.70
Tropics and Southern Hemisphere	0.27	1.04
Total	1.11	2.25

model of the terrestrial biosphere is required. We chose the Carnegie-Ames-Stanford Approach (CASA) model (*19*), because it predicts ecosystem fluxes of CO_2 with a relatively straightforward extrapolation of global satellite imagery (normalized difference vegetation index or NDVI measurements on a 1° grid). We calculated $R(\mathbf{x})$ by running each atmospheric model with surface fluxes from a version of the CASA model (again until a steady state spatial pattern was achieved). To calculate $b_i(\mathbf{x})$, we ran the atmospheric model with no sources or sinks of CO_2 except net primary production (NPP) from the CASA model in only the i^{th} region. This NPP was first rescaled until the annual total was 1 Pg C. Thus, the spatiotemporal distribution of estimated carbon sinks within each terrestrial region is assumed to be proportional to the distribution of NPP, but this assumption has little impact on the results (see below).

The atmospheric CO_2 data we used cover the 1988 to 1992 period at a subset of 63 sampling stations (*20*) taken from the GLOBALVIEW database (*21*) compiled with methods as described by Masarie and Tans (*22*) (Fig. 1). Before 1988 there were fewer sampling stations; a separate study indicates that even with optimal placement, which the present data set does not have, a minimum of about 10 stations per region is necessary to obtain estimates with useful accuracy (*23*).

We first defined three regions, North America north of 15°N, Eurasia–North Africa north of 24°N, and all other land to the south (Fig. 1). Subsequently, North America was separated into temperate and boreal zones at approximately the evergreen–broadleaf ecotone (51°N). Additional divisions lead to prohibitively large estimation errors. In particular, there are insufficient atmospheric stations in the Southern Hemisphere to separate Africa from South America.

North America is constrained by the atmospheric observations on three sides of the continent (Fig. 1); a large North American terrestrial uptake is estimated in all four combinations of atmospheric models with sea-air CO_2 flux data (Table 2). Most of the North American terrestrial uptake (70 to 100%) is estimated to be in the broadleaf region south of 51°N. If the North American terrestrial uptake were zero (that is, all of the Northern Hemisphere's net terrestrial uptake were in Eurasia), the models would predict an average increase of atmospheric CO_2 of more than 0.3 ppm from stations located between 10°N and 60°N in the North Pacific to those in the North Atlantic. A North American terrestrial sink is implied by the data because the observed gradient shows a decrease from North Pacific to North Atlantic of about 0.3 ppm.

We estimated standard deviations for the estimates of terrestrial uptake by propagating independent, identically distributed Gaussian station errors (Table 2). The ellipses in Fig. 2 suggest that the total Northern Hemisphere sink is well constrained, and that the partitioning between North America and Eurasia–North Africa is more weakly constrained. However, the terrestrial carbon sink in North America is sufficiently large to be detected with the present observational and model constraints.

None of these error estimates include systematic errors such as differences between GCTM and SKYHI and between T97 and OBM. We use the differences between estimates from the four models (Table 2) as an admittedly limited assessment of the magnitude of systematic errors. The range of estimates produced by the differences between the models is small for North American uptake and intermediate for Eurasian uptake. Estimates of Eurasia–North African terrestrial uptake obtained with SKYHI are 0.7 to 0.9 Pg C $year^{-1}$ lower than those obtained with GCTM. SKYHI has a more rapid vertical mixing than GCTM and predicts lower fossil CO_2 at stations in the mid-latitude Northern Hemisphere, which implies a lower terrestrial uptake in the region.

The systematic errors are especially large for estimates of the terrestrial uptake in the tropics and Southern Hemisphere, as evidenced by the large differences among the estimates shown in Table 2. The wide range of 2.0 Pg C $year^{-1}$ in these estimates is caused by a combination of factors. Differences between OBM and T97 account for 1.3 Pg C $year^{-1}$ (Table 2). Differences between SKYHI and GCTM account for 0.7 Pg C $year^{-1}$.

An alternative four-region inversion, with only one region in North America but two in Eurasia–North Africa, yields marginal evidence of a weak uptake in boreal Eurasia (0.6 ± 0.4 Pg C $year^{-1}$) with a more uncertain, but generally compensating source in temperate Eurasia (-0.5 ± 0.7 Pg C $year^{-1}$). However, five-region inversions (with separate temperate and boreal regions in both North America and Eurasia–North Africa) were unstable, with standard errors of estimates as large as 1.4 Pg C $year^{-1}$. The only stable regions were temperate and boreal North America and the union of temperate and boreal Eurasia–North Africa, for which terrestrial uptake estimates and errors similar to those in Table 2 were obtained.

Detection of the terrestrial CO_2 uptake in North America and in Eurasia can be improved

Table 2. Estimated terrestrial carbon uptake for 1988 to 1992. Positive terrestrial carbon uptake is a flux out of the atmosphere. GCTM and SKYHI are the two atmospheric GCM models and T97 and OBM are the two air-sea flux estimates used in the inversions (see text).

Source region	Terrestrial uptake (Pg C $year^{-1}$)				SD of the estimate* (Pg C $year^{-1}$)	Mean and summary SE† (Pg C $year^{-1}$)	Forest area (10^9 ha)
	GCTM		SKYHI				
	T97	OBM	T97	OBM			
			Three-region inversion				
North America	1.6	1.7	1.7	1.7	±0.5	1.7 ± 0.5	0.8
Eurasia and North Africa	0.5	0.5	−0.4	−0.2	±0.5	0.1 ± 0.7	1.2
Tropics and Southern Hemisphere	0.1	−1.1	0.9	−0.5	±0.1	−0.2 ± 0.9	2.1
Total	2.2	1.1	2.2	1.1	–	–	–
			Four-region inversion				
North America							
Boreal	0.4	−0.1	0.5	0.1	±0.3	0.2 ± 0.4	~0.4
Temperate	1.2	1.7	1.2	1.3	±0.4	1.4 ± 0.5	~0.4
Eurasia and North Africa	0.6	0.7	−0.4	0.0	±0.5	0.2 ± 0.7	1.2
Tropics and Southern Hemisphere	0.0	−1.3	0.9	−0.4	±0.1	−0.2 ± 0.9	2.1
Total	2.2	1.1	2.2	1.1	–	–	–

*The SD of the estimate was found by assuming that the Gaussian variance equals χ^2/q ($q = 63$) (*10*), and that data errors from different stations are independent. SDs of estimates obtained with T97 include the sampling uncertainty for oceanic CO_2 exchange (*15*), but those obtained with OBM include no oceanic uncertainty. However, the contribution of T97 error to the total uncertainty is small. †This is the mean of the estimates from the four combinations of atmospheric and oceanic models. The SE is $\sqrt{\sigma^2+V^2}$, where σ is the SD from the adjacent column and V is the SD of the four estimates in the first four columns.

with atmospheric measurements within or near the continents. If the North American uptake were zero, the CO_2 mixing ratios over eastern North America should increase by over 2 ppm (Fig. 1), which would make that the best place to detect a source or sink proportional to NPP. Data are available from two extremely tall towers (>400 m) within this region (crosses in Fig. 1) for a period later than the 1988 to 1992 interval considered here. Analyzed with a completely different method, these data are consistent with the existence of a large sink in North America (*24*).

A detailed summary of the present data that constrain the North American sink (Fig. 3) illustrates how near the limit of detection the signal is. The fit of the model to the observations in the optimal case is better than 0.5 ppm at most locations in both the Pacific and Atlantic. Zeroing out the North American sink lowers the Pacific model predictions and raises the Atlantic, thereby reversing the west-to-east gradient from −0.3 to +0.3 ppm (Fig. 3; note particularly that the Atlantic predictions go from being relatively well centered around the observations to having five stations well above the observations). Zeroing out Eurasia raises the model predictions in the Pacific and lowers them in the Atlantic.

We tested the sensitivity of the solutions to individual stations by removing stations one at a time. In all cases the removal of a station had an impact of ≤0.3 Pg C $year^{-1}$, with most being near zero. The exclusion of Sable Island (44°N60°W) from the data set (*20*) does have a substantial impact on the inversion results. Including it in the GCTM-T97 and -OBM inversions reduces the North American terrestrial uptake by 0.4 to 0.5 Pg C $year^{-1}$ and shifts it to Eurasia–North Africa.

The estimate of North American terrestrial uptake was found to be insensitive to large changes in the North Pacific uptake, and only weakly related to the Southern Ocean (south of 54°S) uptake. In contrast, for an incremental change in the temperate North Atlantic sink, the estimate of North American terrestrial uptake changes by ~1.5 times as much in the opposite direction. However, the temperate North Atlantic sink had to be increased by about a factor of 5, from 0.3 to 1.4 Pg C $year^{-1}$, to eliminate the North American sink (*25*).

A large North American terrestrial uptake was estimated consistently for a range of spatiotemporal patterns assumed for the terrestrial uptake (*26*), because subcontinental terrestrial signals are sufficiently smoothed at most of the air-sampling stations (Fig. 1).

Suppose that our mean estimate of the North American terrestrial carbon sink were distributed uniformly over the forest region south of 51°N (Table 2) (*27*); then, the per unit area forest uptake would be 3 to 4 t C ha^{-1} $year^{-1}$. This is in the uppermost range of some independent measurements at local sites (*28*, *29*). A lower estimate on the order of 1 Pg C $year^{-1}$ for the North American terrestrial uptake, which is near the lower error bound of 1 SD (Fig. 2), would be in better agreement with the local measurements. However, even our low estimate is much larger than the 0.2 to 0.3 Pg C $year^{-1}$ uptake estimated on the basis of forest inventory data for North American forests (*30*, *31*), which did not take full account of carbon storage in soils, wetlands, and lakes (*32*).

The terrestrial uptake in North America is at least partly due to regrowth on abandoned farmland and previously logged forests (*30*, *31*). Numerous field and laboratory studies have suggested that terrestrial uptake is currently enhanced by anthropogenic nitrogen deposition [0.2 to 2.0 Pg C $year^{-1}$ globally, with much of this in the Northern Hemisphere (*33*, *34*)], CO_2 fertilization [0.5 to 2.0 Pg C $year^{-1}$ globally, with most of this in the tropics (*33*)], and global warming [mostly in the north temperate zone (*8*, *35*)]. On the other hand, warming might also have reduced terrestrial uptake by enhancing decomposition (*29*, *36*).

Although the inversion results indicate that the North American terrestrial uptake is large enough to be detected with current data and model constraints, its magnitude remains uncertain and its cause unknown. Thus, the immediate implication of our results is the need for additional constraints of four kinds: (i) intensive atmospheric sampling and ecological field studies to indentify the location and cause of North American terrestrial CO_2 uptake; (ii) new atmospheric measurements to constrain estimates for Eurasia, South America, Africa, and Australia; (iii) studies to better characterize oceanic CO_2 uptake, particularly in the Southern Hemisphere; and (iv) reduced uncertainty in atmospheric transport modeling.

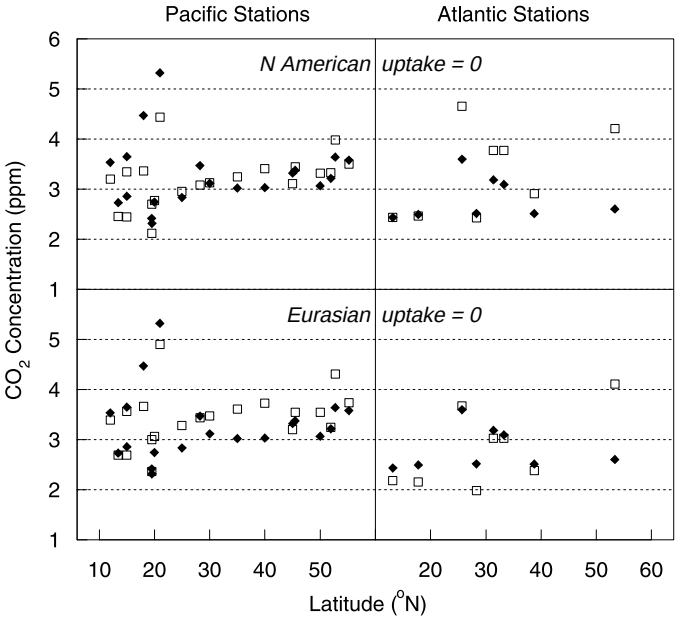

Fig. 3. Comparison of model-predicted atmospheric CO_2 concentrations (□) with observations (1988—1992 average) (◆) at Pacific and Atlantic sampling locations between 10° to 60°N. Model results are shown for GCTM with T97 sea-air fluxes, and with North American terrestrial uptake set to zero (that is, all Northern Hemisphere terrestrial uptake placed in Eurasia–North Africa), or Eurasia–North African terrestrial uptake set to zero (that is, all Northern Hemisphere terrestrial uptake placed in North America). Although the Mace Head station (in the Atlantic at 53.3°N) is an outlier in all plots, it has little impact on the inversion estimates because predictions at this station are affected only slightly by zeroing North American or Eurasian uptake. Data are shown for the following locations, with their latitude (°N) and longitude (a negative sign indicates °W and a positive sign indicates °E) in parentheses: AVI (17.75, −64.75), AZR (38.75, −27.08), BME (32.37, −64.65), BMW (32.27. −64.88), CBA (55.20, −162.72), CMO (45.48, −123.97), CSJ (51.93, −131.02), GMI (13.43, 144.78), IZO (28.30, −16.48), KEY (25.67, −80.20), KUM (19.52, −154.82), MHT (53.33, −9.90), MID (28.22, −177.37), RPB (13.17, −59.43), SHM (52.72, 174.10), STP (50.00, −145.00), pocn15 (15.00, −160.00), pocn20 (20.00, −158.00), pocn25 (25.00, −154.00), pocn30 (30.00, −148.00), pocn35 (35.00, −143.00), pocn40 (40.00, − 138.00), pocn45 (45.00, −131.00), scsn12 (12.00, 111.00), scsn15 (15.00, 113.00), scsn18 (18.00, 115.00), and scsn21 (21.00, 117.00).

References and Notes

1. C. D. Keeling, S. C. Piper, M. Heimann, in *Aspects of Climate Variability in the Pacific and the Western Americas, AGU Monograph 55*, D. H. Peterson, Eds. (American Geophysical Union, Washington, DC, 1989), pp. 305–363.
2. P. P. Tans, I. Y. Fung, T. Takahashi, *Science* **247**, 1431 (1990).
3. I. G. Enting and J. V. Mansbridge, *Tellus* **43B**, 156 (1991).
4. R. M. Law *et al*., *Global Biogeochem. Cycles* **10**, 783 (1996).
5. P. Ciais, P. P. Tans, M. Trolier, J. W. C. White, R. J. Francey, *Science* **269**, 1098 (1995).
6. R. F. Keeling, S. C. Piper, M. Heimann, *Nature* **381**, 218 (1996).
7. R. B. Myneni, C. D. Keeling, C. J. Tucker, G. Asrar, R. R. Nemani, *ibid.* **386**, 698 (1997).
8. C. D. Keeling, J. F. S. Chin, T. P. Whorf, *ibid.* **382**, 146 (1996); J. T. Randerson, M. V. Thompson, T. J. Conway, I. Y. Fung, C. B. Field, *Global Biogeochem. Cycles* **11**, 535 (1997).
9. A. S. Denning, I. Y. Fung, D. Randall, *Nature* **376**, 240 (1995).

10. The sizes of the terrestrial sources and sinks can be estimated by solving for the values of α_j that minimize the sum

$$\chi^2 = \sum_{j=1}^{q} [B(x_j) + O(x_j) + F(x_j) + R(x_j) - S(x_j)]^2 \quad (2)$$

where q is the number of atmospheric sampling stations. In practice, it is convenient to reference all concentrations in the sum of squares to the value at the South Pole, and then solve for the values of α by using singular value decomposition [W. H. Press, B. R. Flannery, S. A. Teukolsky, W. T. Vetterling, *Numerical Recipes* (Cambridge Univ. Press, New York, 1992)] with a mass conservation constraint [G. H. Golub and C. F. V. Loan, *Matrix Computations* (Johns Hopkins Univ. Press, Baltimore, 1990)] that requires the terrestrial biosphere to balance all the other sources minus sinks.

11. J. D. Mahlman and W. J. Moxim, *J. Atmos. Sci.* **35**, 1340 (1978); H. Levy, J. D. Mahlman, W. J. Moxim, *J. Geophys. Res.* **87**, 3061 (1982).
12. Meridional and vertical transport in both GCTM and SKYHI have been evaluated against observations of radon-222, krypton-85, and CFC-11. The original comparison with radon-222 observations led to the implementation of a more aggressive vertical mixing scheme in SKYHI that improved the simulation of this tracer. A recent model comparison study with SF_6 shows that both SKYHI and GCTM do well at simulating marine boundary-layer concentrations, although the continental concentrations may be too high (A. S. Denning *et al*., *Tellus*, in press).
13. K. Hamilton, R. J. Wilson, J. D. Mahlman, L. J. Umscheid, *J. Atmos. Sci.* **52**, 5 (1995).
14. J. L. Sarmiento, R. Murnane, C. L. Quéré, *Philos. Trans. R. Soc. London Ser. A* **348**, 211 (1995); R. Murnane, J. L. Sarmiento, C. L. Quéré, *Global Biogeochem. Cycles*, in press.
15. T. Takahashi *et al*., *Proc. Natl. Acad. Sci. U.S.A.* **94**, 8992 (1997).
16. The sea-air flux is calculated by taking the product of the sea-air pCO_2 difference and a climatic wind speed–dependent estimate of the gas exchange flux based on the oceanic inventory of bomb radiocarbon [R. Wanninkhof, *J. Geophys. Res.* **97**, 7373 (1992)]. Most of the difference between OBM and T97 in global oceanic uptake (0.8 Pg C $year^{-1}$) occurs in the tropics and Southern Hemisphere (Table 1), where the spatiotemporal coverage of measurements used in T97 and tracer data used for model evaluation is very uneven. The recent completion of the World Ocean Circulation Experiment will greatly improve the coverage.
17. U. Siegenthaler and J. L. Sarmiento, *Nature* **365**, 119 (1993).
18. R. J. Andres, G. Marland, I. Fung, E. Matthews, *Global Biogeochem. Cycles* **10**, 419 (1996).
19. C. S. Potter *et al*., *ibid.* **7**, 811 (1993). The CASA model does not consider the effect of biomass burning and biospheric emissions of hydrocarbons. Oxidation of hydrocarbons leads to the formation of CO, which is further oxidized to CO_2 in the atmosphere. Because the biomass burning and CO oxidation sources of CO_2 are not modeled, they are effectively treated here as part of the biospheric respiration of CASA.
20. The GLOBALVIEW-CO2 1996 database has a total of 66 stations. Tae-Ahn Peninsula and Westerland were excluded because they are strongly contaminated by local fossil CO_2 sources that are difficult for the coarse resolution models to simulate in sufficient detail. Sable Island was excluded because it appears that the data may have a positive bias (K. Higuchi, personal communication). The following procedures were followed in calculating annual averages of model simulations for comparison with observations. (i) Sampling of models at coastal stations was moved out to sea by one grid cell in order to avoid inadvertent terrestrial contamination resulting from the coarse resolution of the atmospheric general circulation models (GCMs). (ii) All other sampling was done at the nearest grid cell to the station. (iii) Four stations were sampled by wind sectors in order to match as closely as possible the way that the actual sampling is done: Cape Grim, Tasmania (180° to 270°); Cape Meares, Oregon (210° to 330°); Key Biscayne, Florida (30° to 160°); and Mace Head, Ireland (210° to 300°).
21. GLOBALVIEW-CO2, *Cooperative Atmospheric Data Integration Project—Carbon Dioxide* (NOAA/CMDL, Boulder, CO, 1996), CD-ROM; also available via anonymous FTP to ftp.cmdl.noaa.gov, Path: ccg/co2/GLOBALVIEW.
22. K. A. Masarie and P. P. Tans, *J. Geophys. Res.* **100**, 11,593 (1995).
23. M. Gloor, S.-M. Fan, S. Pacala, J. L. Sarmiento, in preparation.
24. P. S. Bakwin, P. P. Tans, D. F. Hurst, C. Zhao, *Tellus*, in press.
25. The mean North Atlantic air-sea pCO_2 difference measured by T97 is 20 ± 5 μatm. Increasing the temperate North Atlantic air-sea flux to 1.4 Pg C $year^{-1}$ would require an increase in the air-sea pCO_2 difference to about 90 μatm, or a 4.5 times increase of the gas exchange coefficient [which is already about twice as large as other commonly used estimates (*17*)], or some combination of the two. Tans *et al*. discussed this issue in their study (*2*). An independent constraint on the North Atlantic sink is the anthropogenic carbon inventory estimate obtained from analysis of observations of dissolved inorganic carbon [N. Gruber, J. L. Sarmiento, T. F. Stocker, *Global Biogeochem. Cycles* **10**, 809 (1996)]. This estimate is almost identical to the OBM simulations (which agree with T97 in the North Atlantic).
26. There was little impact on the estimates when the terrestrial uptake was assumed to be proportional to the heterotrophic respiration in the CASA model (*19*), which has very different temporal patterns from the NPP. In another case, the terrestrial uptake was assumed to be invariable with season and to be uniform within each of five regions (separate boreal and temperate regions in Eurasia–North Africa and North America, and the rest of land surfaces combined). The estimates of total terrestrial uptake for North America and for Eurasia–North Africa were well constrained and remained essentially unchanged from those shown in Table 2 (averaged over the four cases) even with this radical assumption.
27. M. Williams, in *World Deforestation in the Twentieth Century*, R. J. Richards and R. P. Tucker, Eds. (Duke Univ. Press, Durham, NC, 1988), pp. 211–229; K. Power, personal communication.
28. S. C. Wofsy *et al*., *Science* **260**, 1314 (1993); M. L. Goulden, J. W. Munger, S. M. Fan, B. C. Daube, S. C. Wofsy, *ibid.* **271**, 1576 (1996); S. Greco and D. D. Baldocchi, *Global Change Biol.* **2**, 183 (1996).
29. M. L. Goulden, J. W. Munger, S.-M. Fan, B. C. Daube, S. C. Wofsy, *Science* **279**, 214 (1998).
30. R. A. Birdsey *et al*., *USDA Forest Service, Productivity of America's Forests and Climate Change* (1995); D. P. Turner, G. J. Koerper, M. E. Harmon, J. J. Lee, *Ecol. Appl.* **5**, 421 (1995).
31. D. Schimel *et al*., in *Climate Change 1995*, J. T. Houghton *et al*., Eds. (Cambridge Univ. Press, Cambridge, 1996), pp. 76–86
32. R. F. Stallard, *Global Biogeochem. Cycles* **12**, 231 (1998).
33. J. M. Melillo, I. C. Prentice, G. D. Farquhar, E.-D. Schulze, O. E. Sala, in (*31*), pp. 447–481.
34. D. W. Schindler and S. E. Bayley, *Global Biogeochem. Cycles* **7**, 717 (1993); R. J. M. Hudson, S. A. Gherini, R. A. Goldstein, *ibid.* **8**, 307 (1994); A. R. Townsend, B. H. Braswell, E. A. Holland, J. E. Penner, *Ecol. Appl.* **6**, 806 (1996); E. A. Holland *et al*., *J. Geophys. Res.* **102**, 15849 (1997).
35. N. Nicholls, *et al*., in (*31*), pp. 133–192; R. B. Myneni, S. O. Los, C. J. Tucker, *Geophys. Res. Lett.* **23**, 729 (1996).
36. A. Dai, I. Y. Fung, *Global Biogeochem. Cycles* **7**, 599 (1993).
37. This research was carried out as part of the Carbon Modeling Consortium (CMC), which is supported by the Office of Global Programs and Geophysical Fluid Dynamics Laboratory of the NOAA. We acknowledge support from the Department of Energy. Stimulating discussions with our colleagues in the CMC and elsewhere is gratefully acknowledged, with particular appreciation to P. Bakwin, D. Baker, and M. Bender. L. Bruhwiler, R. Hemler, H. Levy, and W. Moxim provided advice on the GCTM and SKYHI simulations, T. Hughes helped access the OBM results, and C. Field provided the CASA simulation results.

29 May 1998; accepted 15 September 1998

North Atlantic Oscillation Dynamics Recorded in Greenland Ice Cores

C. Appenzeller,* T. F. Stocker, M. Anklin

Carefully selected ice core data from Greenland can be used to reconstruct an annual proxy North Atlantic oscillation (NAO) index. This index for the past 350 years indicates that the NAO is an intermittent climate oscillation with temporally active (coherent) and passive (incoherent) phases. No indication for a single, persistent, multiannual NAO frequency is found. In active phases, most of the energy is located in the frequency band with periods less than about 15 years. In addition, variability on time scales of 80 to 90 years has been observed since the mid-19th century.

The North Atlantic oscillation (NAO) is one of the Northern Hemisphere's major multiannual climate fluctuations and typically is described with an index based on the pressure difference between Iceland and the Azores (*1*). On multiannual time scales, variations in the NAO have a strong impact on North Atlantic and European climate (*2*) and also on the recent surface temperature warming trend in the Northern Hemisphere (*3*). In recent decades the winter index remained predominantly in a positive state, and there is evidence that during this period the variability might have increased (*4*). Analysis of various NAO indices (*5*) showed

C. Appenzeller and T. F. Stocker, Climate and Environmental Physics, University of Bern, Sidlerstrasse 5, CH-3012 Bern, Switzerland. M. Anklin, Department of Hydrology and Water Resources, University of Arizona, Tucson, AZ 85721, USA.

*To whom correspondence should be addressed. E-mail: christof.appenzeller@climate.unibe.ch